Journal of Alloys and Compounds 890 (2021) 161849

Contents lists available at ScienceDirect

Journal of Alloys and Compounds

journal homepage: www.elsevier.com/locate/jalcom

Tailoring the magnetocaloric, magnetic and thermal properties of $Dy_6(Fe,Mn)X_2$ intermetallics (X=Sb, Te, Bi)

A. Herrero[a], A. Oleaga[a,*], I.R. Aseguinolaza[a], A.J. Garcia-Adeva[a], E. Apiñaniz[a], A.V. Garshev[b], V.O. Yapaskurt[c], A.V. Morozkin[b]

[a] Departamento de Física Aplicada, Escuela de Ingeniería de Bilbao, Universidad del País Vasco UPV/EHU, Plaza Torres Quevedo 1, 48013 Bilbao, Spain
[b] Department of Chemistry, Moscow State University, Leninskie Gory, House 1, Building 3, GSP-2, Moscow 119991, Russia
[c] Department of Petrology, Geological Faculty, Moscow State University, Leninskie Gory, Moscow 119991, Russia

ARTICLE INFO

Article history:
Received 30 April 2021
Received in revised form 23 August 2021
Accepted 1 September 2021
Available online 4 September 2021

Keywords:
Magnetocaloric effect
Rare earth compound
Magnetic properties
Spin-ordering
Critical behavior

ABSTRACT

The structural, magnetic, magnetocaloric (MCE) and thermal properties of seven Fe_2P-type $Dy_6(Fe,Mn)X_2$ (X=Sb, Bi, Te) intermetallics (space group $P\bar{6}2m$, N 189, hP9) have been experimentally studied. They present a paramagnetic to ferromagnetic transition (in the range 129–370 K), followed, as temperature decreases, by a spin-reorientation one (from 52 to 170 K) and a ground magnetic state at 2 K with antiferromagnetic components. This state turns into a ferromagnetic state when a magnetic field is applied. The critical exponents β,γ,δ related to the PM-FM transition point to long range order interactions but in most compounds their values severely deviate from the Mean Field class, presenting an unconventional critical behavior, probably due to magnetocrystalline anisotropies. This magnetic complexity has the consequence that in every intermetallic three MCE effects arise: Two direct magnetocaloric effects (DMCE) with a table-like effect in between (from 40 K to more than 400 K), with moderate values of the magnetic entropy maxima (up to 6.9 J/kgK for $\mu_0\Delta H$ = 5 T, with the tableau in-between being around 4 J/kgK, for Dy_6FeSb_2 and $Dy_6FeSbTe$). The calculation of the Thermal Average Entropy Change allows to place the properties of two compounds (Dy_6FeSb_2 and $Dy_6FeSbTe$) close to other rare earth based high entropy alloys described in literature. The seven compounds present a relevant third MCE, inverse, below 25 K, with a value as high as 17.8 J/kgK ($\mu_0\Delta H$ = 5 T) for $Dy_6FeSbTe$. The maximum of the magnetic entropy change at the Curie temperature has been shown to scale with the critical exponents found and universal curves have been built. Finally, the thermal diffusivities in the range of the DMCE have been measured, with the result that they present good values (between 1 and 3 mm^2/s) to be used in real magnetocaloric refrigeration systems.

1. Introduction

Magnetic refrigeration is a constantly expanding field searching for new technological devices which can effectively substitute the gas compressor-expansion based devices [1–3] in the different temperature ranges of interest: room temperature is the most obvious one but the different gas liquefaction regions are extremely interesting as well [4–8]. Therefore, there is a constant search for materials with relevant magnetocaloric properties. In order for this kind of materials to be of practical interest in real applications, they must combine a high magnetic entropy change at the desired temperature with a high value of the refrigerant capacity. This can be accomplished by either manufacturing composite materials presenting close phase transitions, or by selecting a single material with several magnetic transitions close enough to maintain a tableau in the magnetic entropy change among all of them, therefore spanning the temperature range of application. As the magnetocaloric materials will work in a cycle in a refrigeration system, it is desirable to avoid hysteresis (magnetic and thermal). To this end, one research option is to focus on materials with a first order magnetic transition, which usually gives high values of the magnetic entropy change, and try to reduce the hysteresis by manipulating the composition or the microstructure while maintaining good magnetocaloric properties [9–12]; another line is to work on second order phase transitions and try to improve the performance by playing with the stoichiometry in order to obtain table-like magnetocaloric effects over the desired temperature range, combining two (or more) phase transitions; this is the case of many rare earth based materials [4,13–15]. This approach is very interesting because an ideal Ericsson

* Corresponding author.
E-mail address: alberto.oleaga@ehu.es (A. Oleaga).

https://doi.org/10.1016/j.jallcom.2021.161849
0925-8388/

refrigeration cycle (consisting on two isothermal and two isofield processes) requires a constant value of the magnetic entropy change (ΔS_M) in order to obtain the maximum efficiency and optimal performance [2]. A last aspect of interest is to be able to broadly tune the working temperature range to cover the gas liquefactions ranges.

Finally, an aspect seldom taken into account when designing new magnetocaloric materials concerns the thermal properties: The heat exchange between the magnetocaloric material and the fluid in the refrigerator must be efficient and quick, allowing high working frequencies. Though in some cases in literature the thermal conductivity has been measured [3], the really relevant property is the thermal diffusivity as it is a non-steady heat transfer situation [16].

This work focuses on the development of the general family R_6TX_2, with R =rare earth, T = Fe, Mn and X = Sb, Te, Bi, as many members of this family present two magnetic transitions with relevant magnetocaloric properties, building a table-like figure in between. We already showed in previous works that the combination $(Gd,Tb)_6(Fe,Mn)Bi_2$ allowed to tune a broad MCE around room temperature while $Ho_6(Mn,Fe)Bi_2$ could cover a region between 40 and 250 K [14,15]. Besides, the magnetic properties of this family are quite complex, which is extremely interesting in itself. Most compounds present a paramagnetic to ferromagnetic (PM-FM) transition at a certain temperature, followed by a second one (as temperature is lowered) where the spins are reoriented leading to complex non-collinear spin arrangements. In addition, at even lower temperatures, metamagnetic transitions arise to reach a clear ferromagnetic state. The study of the critical behavior of the PM-FM transitions in all compounds, obtaining the critical exponents (β,γ,δ,n), will give a broader knowledge of the magnetism of these compounds, as they are related to the range of the magnetic interactions, the dimensionality of the system and the spins arrangement. Besides, it is possible to predict the magnetocaloric behavior of the system at not measured fields with the previous knowledge of these critical parameters.

The current work focuses on Dy-based compounds not studied before, with the aim of extending the knowledge of the complexity of the magnetic properties, and the possible displacement of MCEs both to lower and higher temperatures; at the same time, the study of the influence on all properties of the substitution of the last element (X = Sb, Te, Bi) is introduced for the first time. The purpose is to study the possibility of optimizing the magnetic and magnetocaloric properties. Concerning the applications in the low temperature ranges, the fact that the samples with Tb showed in that region an inverse magnetocaloric effect foretells that Dy might have a similar effect, which could be tuned with different combination of ions to become of practical interest.

Therefore, the crystallographic, magnetic, magnetocaloric and thermal properties of seven compounds of the family $Dy_6(Fe,Mn)X_2$ (X=Sb, Te, Bi) will be presented in this study.

2. Samples and experimental techniques

Dy_6FeBi_2, $Dy_6Fe_{0.5}Mn_{0.5}Bi_2$, Dy_6MnBi_2, Dy_6FeSb_2, $Dy_6FeSbBi$, $Dy_6FeSbTe$, and $Dy_6FeBiTe$ alloys with a total mass of 2.5 g were prepared by arc-melting in an electric arc furnace (90 V, 150 A) under argon (99.992 vol%) using a non-consumable tungsten electrode and on a water-cooled copper hearth. Pieces of dysprosium (99.9 wt%), iron, manganese (99.95 wt%), tellurium, antimony and bismuth (purity 99.99 wt%) with some surplus for dysprosium (0.05 g), manganese (0.015 g), tellurium (0.05 g), antimony (0.02 g) and bismuth (0.03 g) were used as starting components. A titanium button was used as a getter during arc-melting and the alloys were re-melted three times. The arc-melted samples were wrapped into nickel foil and sealed in silica ampoules, evacuated and back filled with argon to 0.3 atm at room temperature. The samples were annealed at 1070 K (± 2 K) for 340 h, then quenched in ice-water bath.

Phase analysis of the alloys was carried out using X-ray diffraction and energy dispersive X-ray spectroscopy microprobe elemental analysis (EDS). The X-ray powder data (XRD) were obtained by using a diffractometer Rigaku D/MAX-2500 (CuKα, 2θ of 10–80°, 0.02° step, Imax/Ibgr ~30–40). An INCA-Energy-350 X-ray EDS spectrometer (Oxford Instruments) on a Jeol JSM-6480LV scanning electron microscope (SEM) (20 kV accelerating voltage, 0.7 nA beam current and 50 µm beam diameter, microprobe size ~ 10 nm) was employed to perform quantitative elemental analysis. Signals averaged over three points per phase gave estimated standard deviations of 0.5 at% for dysprosium (measured by L-series lines), 1 at% for Mn and Fe and 0.6 at% for Sb, Bi and Te (measured by K-series lines).

The unit cell data were derived from powder X-ray data using the Rietan-program [17] in the isotropic approximation at room temperature.

The magnetic properties have been measured using a Vibrating Sample Magnetometer (VSM) by Cryogenic Limited, retrieving the magnetization M of the samples under external applied magnetic fields H_a in the range of 0–7 T. Magnetization isotherms have been collected from 2 K to temperatures well above the corresponding Curie temperature T_C, using a discontinuous protocol in the regions where metamagnetic transitions have appeared, in order to erase the magnetic memory of the samples and be able to extract the magnetic entropy change using the well known Maxwell relation in order to avoid spurious results [18]. The step between magnetization isotherms has been varied depending on the temperature range of measurements, being ΔT = 1 K around T_C. Demagnetization effects have been taken into account in order to perform a correct evaluation of the scaling analysis and the magnetocaloric effect [19], thus obtaining the internal magnetic field $H_i = H_a - NM$, where N is the demagnetization factor, which has been obtained from zero-field *ac* susceptibility measurements following the method described in [20]. The magnetic susceptibility was measured with AC Measurement System Option in PPMS (Physical Properties Measurement System) by Quantum Design. In all the figures in this study the symbol H has been used to denote H_i, in order to simplify the notation.

Finally, thermal diffusivity has been measured using a high resolution *ac* photopyroelectric calorimeter in the back detection configuration [21].

3. Experimental results and discussion

3.1. Structural data and phase analysis

The X-ray powder analysis (see supplementary Fig. 1s) showed that the already known Dy_6FeBi_2, Dy_6MnBi_2, Dy_6FeSb_2 ternary compounds [22–25] and the novel $Dy_6Fe_{0.5}Mn_{0.5}Bi_2$, $Dy_6FeSbBi$, $Dy_6FeSbTe$ and $Dy_6FeBiTe$ quasiternary solid solutions crystallize in the Fe_2P-type structure (space group $P\bar{6}2m$, No. 189, $hP9$). The refined unit cell data and atomic positions are given in Table 1. The replacement of Sb for Bi, Sb for Te, Bi for Te and Fe for Mn in $Dy_6\{Fe, Mn\}\{Sb, Bi, Te\}_2$ compounds [22–25] should follow via a monotonic distortion of the unit cell, which is confirmed via the cell parameters of $Dy_6FeSbTe$, $Dy_6FeSbBi$, $Dy_6FeSbBiTe$ and $Dy_6Fe_{0.5}Mn_{0.5}Bi_2$ solutions (see Fig. 1).

Generally, the type of rare earth, the set of interatomic distances in the rare earth sublattice and the magnetic catalysis of .Mn-Mn-Mn. chains (shortest Mn-Mn distance is the same as c cell parameter) determine the magnetic ordering of Fe_2P-type compound [26], which is observed for magnetic ordering of present quasiternary $Dy_6FeSbTe$, $Dy_6FeSbBi$, $Dy_6FeBiTe$ and $Dy_6Fe_{0.5}Mn_{0.5}Bi_2$.

The prepared alloys contain an admixture of Yb_5Bi_3-, Yb_5Sb_3-, NaCl- and $MgCu_2$-type phases [27] (1–9 wt%) (see supplementary Table 1s, which contains the analysis of secondary phases for each compound). The possible influence of these admixture phases in the

Table 1
Unit cell data of Fe_2P-type Dy-containing compounds (space group $P\bar{6}2m$, N 189, *hP*9).

Compound	*a* (nm)	*c* (nm)	*c*/*a*	*V* (nm3)	RF (%)	Ref.
Dy_6FeBi_2	0.82494(6)	0.41899(3)	0.50790	0.24693	5.1	**a-**
	0.82441	0.41885	0.50806	0.24653		[23]
$Dy_6Fe_{0.5}Mn_{0.5}Bi_2$	0.82414(6)	0.42284(3)	0.51307	0.24872	5.1	**a-**
Dy_6MnBi_2	0.82204(7)	0.42929(3)	0.52223	0.25123	5.4	**a-**
	0.82298	0.42762	0.51960	0.25082		[24]
Dy_6FeSb_2	0.81383(6)	0.41651(3)	0.51179	0.23890	5.1	**a-**
	0.8138	0.4151	0.51008	0.23808		[22]
$Dy_6FeSbBi$ **b-**	0.81930(6)	0.41775(3)	0.50989	0.24285	3.4	**a-**
$Dy_6FeSbTe$	0.81906(6)	0.40883(3)	0.49915	0.23752	5.8	**a-**
$Dy_6FeBiTe$	0.82433(7)	0.41045(3)	0.49792	0.24154	6.2	**a-**
Dy_6FeTe_2	0.8236	0.40102	0.48691	0.23558		[25]

a- this work; b- Dy1 3 g [0.5985(5), 0, 1/2], Dy2 3 f [0.2388(5), 0, 0], Fe 1b [0, 0, 1/2], Sb0.5Bi0.5 2c [1/3, 2/3, 0], atomic displacement parameters of all atoms β11 = β22 = 0.004966, β12 = 0.002483, β33 = 0.014325 (β11 = β22 = B11/[3a2], β12 = B11/[6a2], β33 = B33/[2c]2).

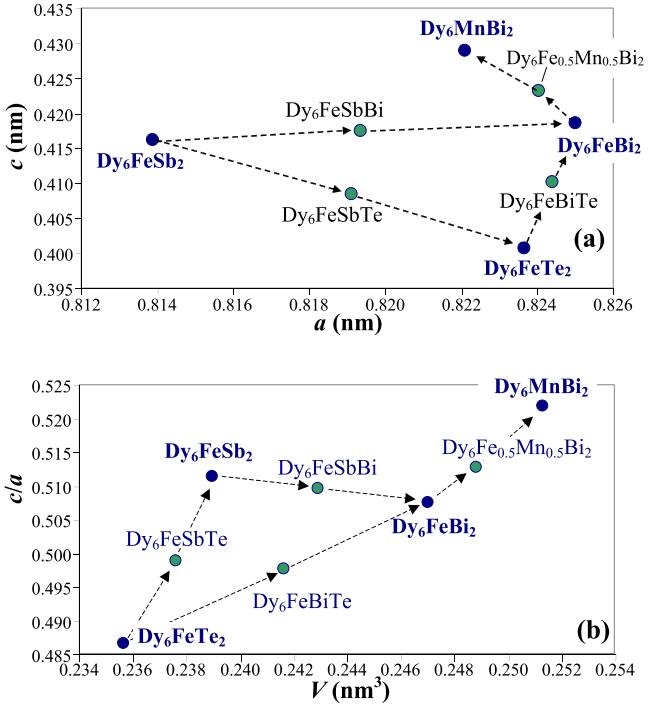

Fig. 1. Unit cell data of Fe_2P-type ternary Dy_6FeTe_2, Dy_6FeSb_2, Dy_6FeBi_2 and Dy_6MnBi_2 compounds and $Dy_6FeSbTe$, $Dy_6FeBiTe$, $Dy_6FeSbBi$ and $Dy_6Fe_{0.5}Mn_{0.5}Bi_2$ quasiternary solid solutions: (a) cell parameter *c* vs cell parameter *a* and (b) *c*/*a* ratio vs unit cell volume *V*.

magnetic properties of Fe_2P-type compounds will be considered in the next section. Finally, Fig. 2 shows an example of the microstructure of several samples obtained by EDS analysis.

3.2. Magnetic characterization

In this section we will locate and characterize the different magnetic transitions from 2 K to the paramagnetic state in all samples/alloys, by means of the magnetization as a function of temperature, the *ac* susceptibility, and the general behavior of the magnetization isotherms as a function of the applied field.

Fig. 3 shows the magnetization as a function of temperature, both in Zero-Field Cooled (ZFC) and Field-Cooled (FC) mode for a selection of compositions (the rest are included in Fig. 2s in the Supplementary material). In all cases there is a strong difference between the FC and ZFC curves, denoting thermomagnetic irreversibility, typical of many ferromagnetic transitions. In particular, in a previous work with $Tb_6(Fe,Mn)Bi_2$ a similar behavior was observed [15], which is no surprising, as the presence of Tb or Dy in many other families produce some common magnetic features [21,28]. The real part of the *ac* susceptibility is a very precise indicator of the location of the different transitions and it is collected in Fig. 4. In all cases there is a paramagnetic to ferromagnetic (PM-FM) transition at a certain temperature T_C which ranges from 364 K in Dy_6MnBi_2 to 128 K in $Dy_6FeBiTe$, and which commonly leads to a collinear magnetic structure of the rare earth spins in R_6TX_2 [25,26,29–31]. Besides, in all cases there is another transition at a lower temperature T_m (from about 148 K in Dy_6MnBi_2 to 56 K in Dy_6FeSb_2) which, in the R_6TX_2 family, is due to a reorientation of the rare earth spins leading to complex non-collinear spin arrangements, including canted ferromagnets, conical or spiral or simply antiferromagnetic [25,26,29–32]. So far, no magnetic moment has been found for the transition metal in this intermetallic family [26,31,32].

There is a good agreement in the position of T_C for Dy_6FeBi_2 and T_m for Dy_6MnBi_2 with literature, which are the only ones previously measured [26]. Regarding the PM-FM transition and starting from Dy_6FeBi_2, we can see in Fig. 4 that the substitution of Fe by 50% Mn takes T_C about 120 K higher, while a complete substitution increases its value more than 100 additional degrees. This further confirms the possibility of tuning the position of this transition by playing with the Mn composition, as seen before in other members of $R_6(Fe,Mn)Bi_2$ [14,15,26,29,33]. On the other hand, the substitution of Bi in Dy_6FeBi_2 by Sb and Te (totally or partially) leads to a small displacement of just several degrees in T_C. Finally, it is worth noting that the effect of these substitutions is much stronger in the magnetic properties in the region of the spin reorientation transition, not only in the displacement of T_m but also in the shape of the curves with even an additional reorientation transition in Dy_6FeSb_2 at 11 K.

The presence of secondary phases affects very little the magnetic properties of the main phases. Dy_5Bi_3 is present in two samples: $Dy_6Fe_{0.5}Mn_{0.5}Bi_2$ and Dy_6MnBi_2. It is known that it has a ferromagnetic transition at 50 K [34] but nothing can be appreciated at that temperature in $Dy_6Fe_{0.5}Mn_{0.5}Bi_2$ and, in Dy_6MnBi_2, there is only a small peak at 58 K but it is not evident if it belongs to that phase or to the main one. Dy_5Sb_3, which presents an antiferromagnetic transition at 69 K [35], is present in Dy_6FeSb_2, and it could be superimposed on the right hand side of the peak in χ'_{ac}, which marks the strong reorientation transition which takes place at about 50 K. It is worth noting a second reorientation transition in Dy_6FeSb_2, at 11 K, which can not be attributed to a secondary phase. Finally, the secondary phases in $Dy_6FeSbBi$, $Dy_6FeSbTe$ and $Dy_6FeBiTe$ have not been magnetically characterized yet so they could be responsible for some features such as the elbow in $Dy_6FeSbBi$ on the lower temperature side of T_m but the general aspects of the curves tell that they do not have much relevance, if any.

The order of the magnetic transitions can be evaluated by means of the Banerjee criterion [36] which states that, in the representation of M^2 versus (*H*/*M*), the slopes of the curves must be positive if the transition is continuous while there should be regions with negative slopes if it were a first order one. Fig. 5 shows, for the case of the spin

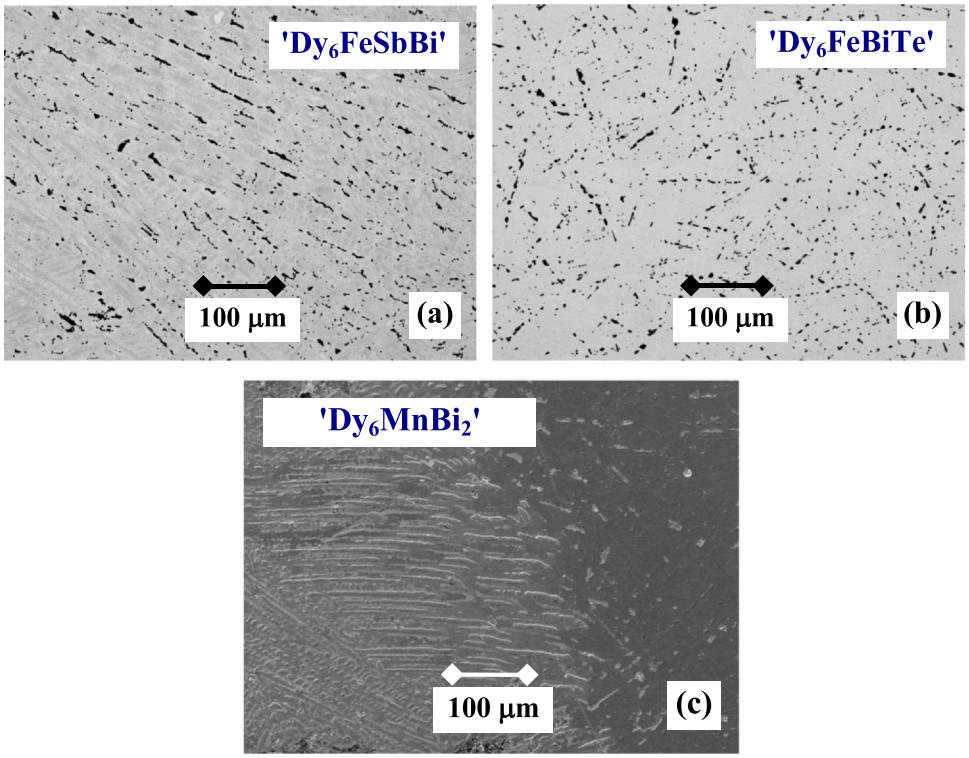

Fig. 2. Microstructure of (a) 'Dy$_6$FeSbBi': Dy$_{66.3(4)}$Fe$_{10.9(8)}$Sb$_{11.3(4)}$Bi$_{11.5(4)}$ (Fe$_2$P-type) (grey phase), Dy$_{62.0(6)}$Fe$_{3.8(8)}$Sb$_{19.1(5)}$Bi$_{15.1(4)}$ (Yb$_5$Sb$_3$-type) (white phase) and Dy$_{32.5(8)}$Fe$_{67.1(9)}$Bi$_{0.4(4)}$ (MgCu$_2$-type) (black phase), **(b)** 'Dy$_6$FeBiTe': Dy$_{66.3(6)}$Fe$_{11.1(8)}$Bi$_{12.1(6)}$Te$_{10.5(8)}$ (Fe$_2$P-type) (grey phase), Dy$_{66.8(9)}$Bi$_{0.9(8)}$Te$_{32.3(8)}$ (Sc$_2$Te-type) (black phase), Dy$_{50.8(8)}$Bi$_{24.9(6)}$Te$_{24.3(6)}$ (NaCl) (black phase) and (c) 'Dy$_6$MnBi$_2$': Dy$_{67.2(7)}$Mn$_{10.7(8)}$Bi$_{22.1(6)}$ (Fe$_2$P-type) (grey/dark grey phase), Dy$_{64.7(6)}$Bi$_{35.3(8)}$ (Yb$_5$Bi$_3$-type) (white-grey phase).

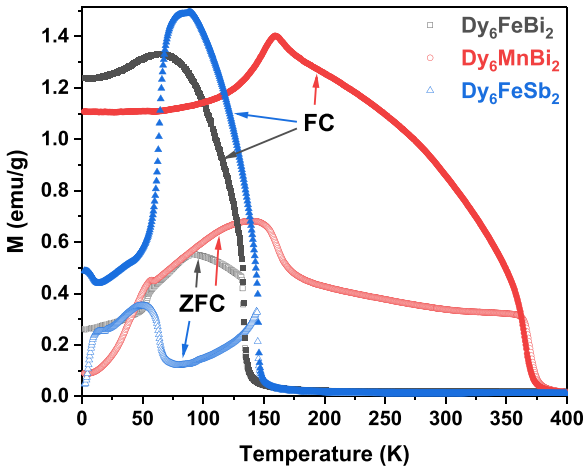

Fig. 3. Magnetic moment as a function of temperature in zero-field cooled (ZFC, open symbols) and field-cooled (FC, closed symbols) mode with applied field H = 10 Oe for Dy$_6$FeBi$_2$, Dy$_6$MnBi$_2$, Dy$_6$FeSb$_2$.

reorientation transition (T_m) in Dy$_6$FeSbTe and the PM-FM transition (T_C) in Dy$_6$FeBiTe, how all slopes are positive, confirming that they are second order transitions. This happens in the seven compounds for these transitions. This behavior will be further confirmed by the thermal diffusivity measurements shown in Section 3.5.

The thermomagnetic irreversibility appreciated in Fig. 3 and Fig. 2s is easily understandable when the isothermal magnetization loops at 2 K are analysed (see Fig. 6). In all cases there is not only a coercive field H_C but also step-like behaviors characteristic of metamagnetic transitions, from ground states with antiferromagnetic components responsible for non-collinear magnetic structures, to ferromagnetic states.

If the magnetization isotherms are analysed, the following common properties can be ascertained (which are shown for some of them in Fig. 7): from 2 K to a certain temperature value (50 K for Dy$_6$FeBi$_2$, 36 K for Dy$_6$Fe$_{0.5}$Mn$_{0.5}$Bi$_2$, 28 K for Dy$_6$MnBi$_2$, 20 K for Dy$_6$FeSb$_2$, 30 K for Dy$_6$FeSbBi, 26 K for Dy$_6$FeSbTe, and 30 K for Dy$_6$FeBiTe) the magnetization increases from one isotherm to the next one (in ascending order) for the same value of the magnetic field, assessing the existence of antiferromagnetic interactions in those temperature ranges. For higher temperatures, the ferromagnetic behavior imposes, which means that, for a given applied field, the magnetization decreases as temperature is increased. Of course, in the low temperature ranges the metamagnetic transitions are clearly observed for all samples. In some cases it quickly disappears with the applied field at very low temperatures, reaching a ferromagnetic state.

3.3. Critical behavior

As stated in the introduction, the study of the critical behavior of second order magnetic phase transitions provides information about the range of the magnetic interactions, the dimensionality of the system and the spins arrangement. This study has been performed on the PM-FM phase transitions in all compounds. In this section we will extract the critical exponents (β,γ,δ) which are associated to the singular behavior of the spontaneous magnetization M_S, the initial susceptibility χ^0 and the critical isotherm, respectively, in a region close to T_C, following the equations [37]:

$$M_S(T) \sim |t|^{\beta} \ (T < T_C), \tag{1}$$

$$\chi_0^{-1}(T) \sim |t|^{\gamma} \ (T > T_C), \tag{2}$$

$$M(H) \sim H^{1/\delta} \ (T = T_C), \tag{3}$$

where $t = (T-T_C)/T_C$ is the reduced temperature; the magnetic equation of state

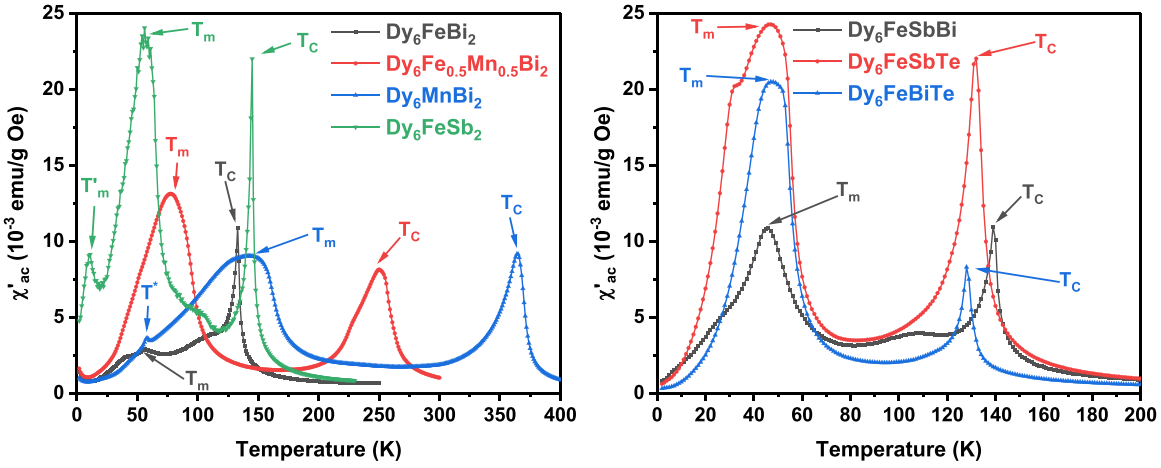

Fig. 4. Real part of the *ac* susceptibility at $f = 100$ Hz. T_C corresponds to the paramagnetic to ferromagnetic transitions, T_m to the spin reorientation ones, T^* to ferromagnetic transitions of the secondary phases.

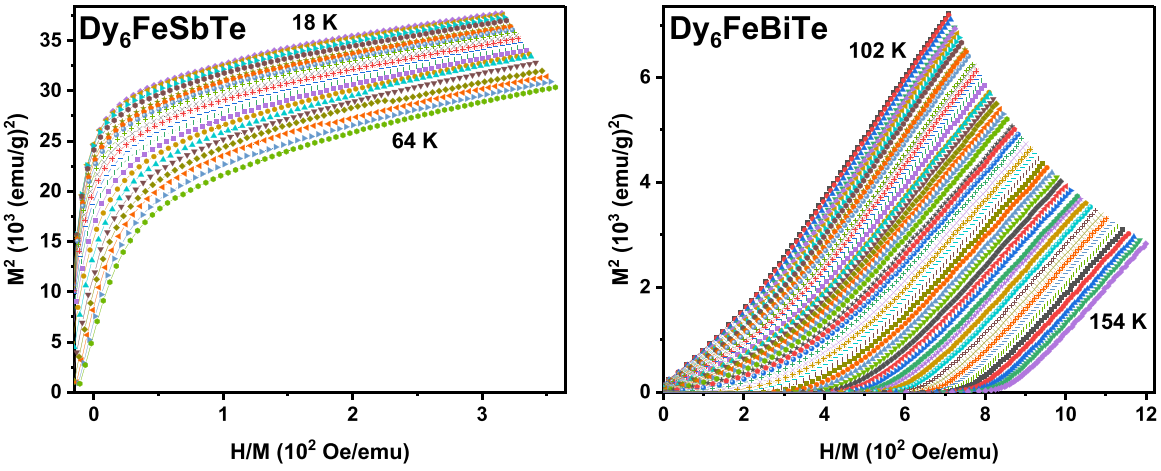

Fig. 5. M^2 as a function of (H/M) around the spin reorientation transition (T_m) in $Dy_6FeSbTe$ and around the PM-FM transition (T_C) in $Dy_6FeSbTe$.

$$M(H, t) = |t|^{\beta} f_{\pm}(H/|t|^{\beta+\gamma}) \quad (4)$$

must be also fulfilled in the critical region. A fourth exponent n, which is related to the magnetocaloric properties, will be considered in Section 3.4.

Detailed magnetization isotherms have been measured in the neighbourhood of the respective Curie temperatures and then the Modified Arrot plots (MAP, $M^{1/\beta}$ represented versus $(H/M)^{1/\gamma}$) have been built up for the most common universality classes in three dimensions (Mean Field, 3D-Heisenberg, and 3D-Ising). If any of the MAP gives straight, parallel lines at high fields, then the critical exponents describing the transition would be the ones associated to that particular universality class (the theoretical values are collected in Table 2 [37–45]). Commonly, as this is not the perfect case, the

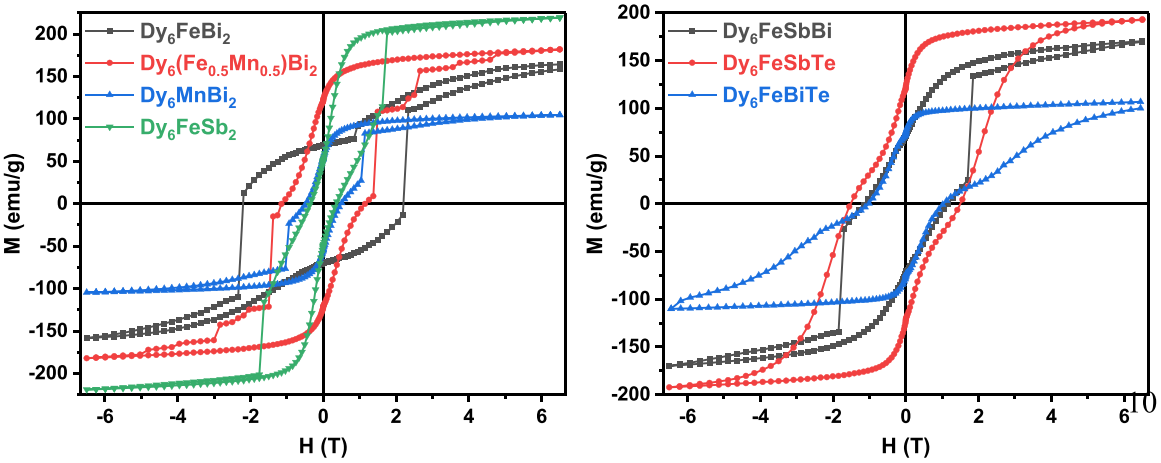

Fig. 6. Isothermal magnetization loops at 2 K for Dy_6FeBi_2, $Dy_6Fe_{0.5}Mn_{0.5}Bi_2$, Dy_6MnBi_2, Dy_6FeSb_2, $Dy_6FeSbBi$, $Dy_6FeSbTe$, and $Dy_6FeBiTe$.

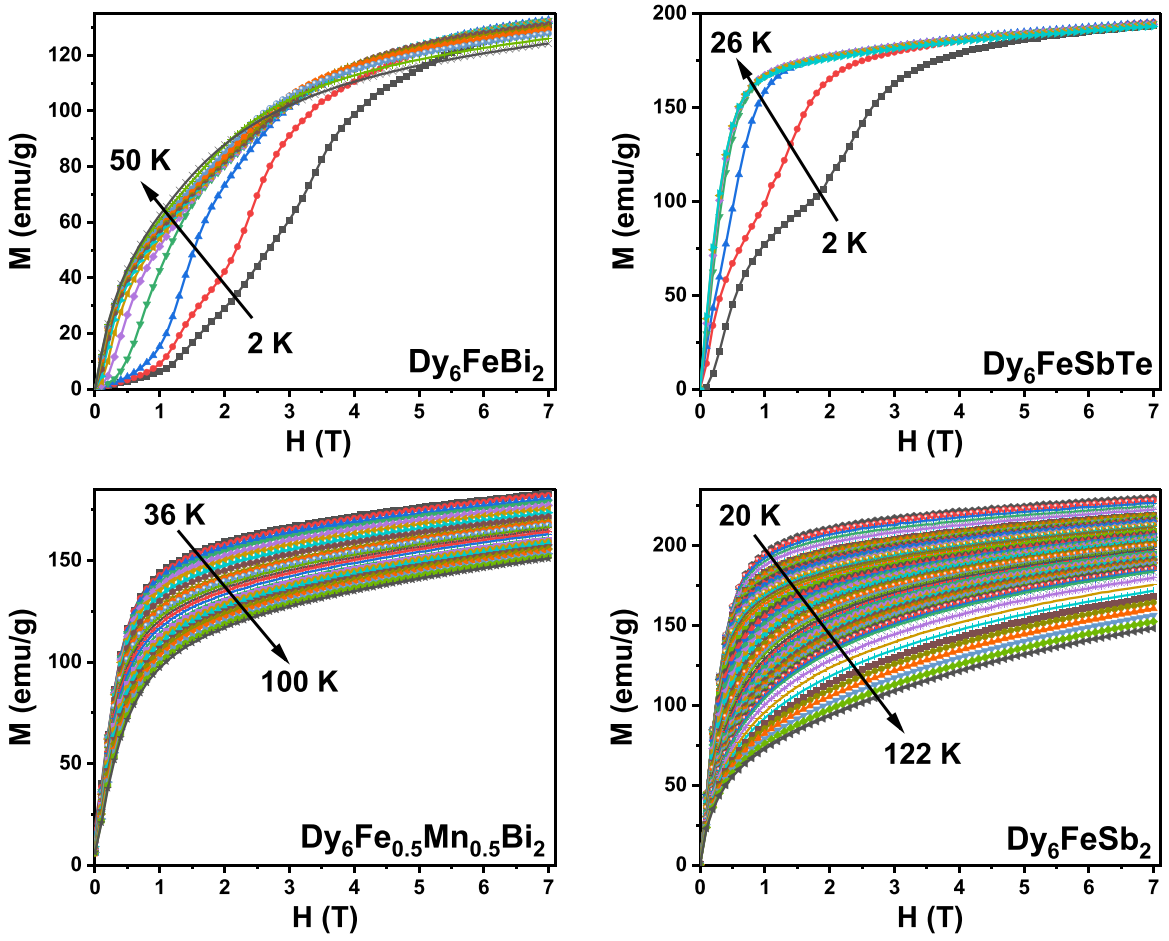

Fig. 7. Magnetization isotherms at low temperature for Dy_6FeBi_2 and $Dy_6FeSbTe$; and at medium temperature for $Dy_6Fe_{0.5}Mn_{0.5}Bi_2$ and Dy_6FeSb_2.

class which gives a closer set of straight, parallel lines at high fields, is taken as a starting point to adjust the particular values of the best critical exponents. A linear extrapolation from high field data on the MAP is then used to extract the $(M_S)^{1/\beta}$ and $(\chi_0^{-1})^{1/\gamma}$ values as the interception with the axes. Once $M_S(T)$ and $\chi_0^{-1}(T)$ are obtained they are fitted to Eqs. (1) and (2) to obtain new values of β and γ. Then, the MAP is again represented until good parallel, straight lines, are obtained in it. But in this family, only for two of them (Dy_6MnBi_2 and $Dy_6FeSbTe$) the Mean Field was a good starting point while for the rest neither of the three classes was close to that situation. So different sets of (β,γ) had to be taken as starting points to finally find good critical exponents which could give straight parallel lines in the Modified Arrott plots.

Table 2
Set of magnetic critical exponents for several universality classes. *d* dimensionality of the interaction, *N* number of spin components, β of spontaneous magnetization, γ of isothermal susceptibility, δ of critical isotherm, n of the magnetic entropy change maximum [37–45].

Universality class	*d*	*N*	*β*	*γ*	*δ*	*n*
Mean-field Model			0.5	1.0	3.0	0.666
2D-Ising	2	1	0.125	1.75	15	0.533
3D-Ising	3	1	0.3265	1.237	4.79	0.569
3D-XY	3	2	0.348	1.317	4.78	0.608
3D-Heisenberg	3	3	0.369	1.396	4.78	0.642
Chiral XY	3	2	0.253	1.13	5.47	0.460
Chiral-Heisenberg	3	3	0.30	1.17	4.90	0.524
Tricritical Mean Field			0.25	1.0	5.00	0.400
2D-Long range	2	1	0.298	1.393	5.67	0.585
3D-Ising spin glass	3	1	0.5	2.9	6.80	0.853

The value of δ is obtained from the fitting of the critical isotherm, after Eq. (3), and then compared with the one using the Widom scaling equation [37]:

$$\delta = 1 + \gamma/\beta \tag{5}$$

The final validation of the critical exponents thus obtained is the fulfilment of the magnetic equation of state Eq. (4): all isotherms must collapse onto two independent branches, one for those below T_C, a second one for those above it.

Fig. 8 shows the curves for the case of $Dy_6FeSbTe$ while the other compositions are shown in Figs. 3s-8s in the Supplementary material, and Table 3 contains the critical exponents with their errors.

In nearly all cases the fittings are very good, with the exception of $Dy_6FeBiTe$. The obtained values of β and γ give in the MAPs a set of straight, parallel curves. The value of δ obtained from the critical isotherm and the one calculated from Eq. (5) are very close and in the representation of the magnetic equation of state all curves collapse onto two independent branches. All of these facts support the validity of the critical exponents found. As mentioned, the values obtained for $Dy_6FeBiTe$ are not so good, as the region in the MAP where the curves are straight and parallel is a short one.

Turning our attention to the particular values of the critical exponents (Table 3) and the theoretical values for a number of universality classes (Table 2) we can see that for Dy_6MnBi_2 (β_{exp} = 0.522, γ_{exp} = 0.93) and $Dy_6FeSbTe$ (β_{exp} = 0.51, γ_{exp} = 0.95) the results are very close to the Mean Field Model (β_{MF} = 0.5, γ_{MF} = 1). This indicates that long range order magnetic interactions are responsible for the transition, but in the rest the values are too high for β (from 0.72 in

Dy_6FeSb_2 to 0.82 for $Dy_6FeBiTe$) to comply with any theorized universality class. On the other hand, in three cases, γ takes values far away from the Mean Field class (0.85 in Dy_6FeSb_2, 0.776 in $Dy_6FeSbBi$, and 0.774 in Dy_6FeBi_2). This situation has already been observed in other close members of this family: Tb_6FeBi_2 (β_{exp} = 0.73, γ_{exp} = 0.80) and $Tb_6Fe_{0.5}Mn_{0.5}Bi_2$ (β_{exp} = 0.72, γ_{exp} = 0.95) [15]. Since the range of the exchange interaction $J(r)$ is mainly determined by the critical parameter γ [46] and the theoretical values for short range order interactions in three dimensions (d=3) are always above 1 (see Table 2), while the values in this case are below that figure, this would suggest that in the samples with Dy the magnetic interactions are long-range, as it happens with those with Tb [15]. The β values above 0.5 imply, for certain, a deviation from the Mean Field model, maybe associated with magnetocrystalline anisotropies due to crystal field effects and a non-zero orbital moment (L=5) of the Dy ion [47]. Even if we explore the possibility of these materials behaving as layered ones (d=2 in Table 2) we see that the critical exponents obtained agree much better with three dimensional models, as the theorized β is much smaller than 0.5 for d = 2 and γ much bigger than 1.

There is a growing amount of materials which do not show a conventional critical behaviour, such as κ-(BEDT-TTF)$_2$X [48], $BaIrO_3$ [49], Mn_3CuN [50], TDAE-C_{60} [51], $Sr_{1-x}A_xRuO_3$ [52,53], $La_{0.4}Ca_{0.6}MnO_3$ [54], and $La_{0.5}Ca_{0.4}Ag_{0.1}MnO_3$ [55]. This points to the fact that there might be other universality classes still to be developed which could properly describe the magnetism in these materials, an issue which should be addressed by theoretical research groups.

3.4. Magnetocaloric properties

The magnetic entropy change $\Delta S_M$and the refrigerant capacity have been evaluated in the respective temperature ranges of interest, with the limit that it has not been possible to perform measurements over 400 K. The well known Maxwell equation has been used to indirectly obtain ΔS_Mas a function of temperature and magnetic field

$$\Delta S_M(T, \Delta' H) = \mu_0 \int_{H_i}^{H_f} \left(\frac{\partial M}{\partial T}\right)_H dH \quad (6)$$

The results are shown in Fig. 9 and the maxima at each transition are collected in Table 4. The magnetocaloric properties of this family are extremely rich as, in all cases, there are two direct magnetocaloric effects (DMCE) whose superposition in-between allows the maintenance of a table-like MCE effect over a wide temperature range, which is required for an ideal Ericsson refrigeration cycle. Besides, there is a strong inverse magnetocaloric effect (IMCE) at very low temperatures. The highest temperature DMCE is associated with the PM-FM transition while the second DMCE is due to the spin reorientation transition. The highest values of $|\Delta S_M^{pk}|$are, for $\mu_0\Delta H \sim 7$ T, 9 J/kgK for the two DMCE effects in Dy_6FeSb_2 and one of the DMCE for $Dy_6FeSbTe$, with the tableau in-between being 6–7 J/kgK for those compositions. It is clear from Fig. 9 that the role of Fe-Mn is to move the operational region for a refrigeration device in a very broad temperature range (from 40 K to more than 400 K) while the

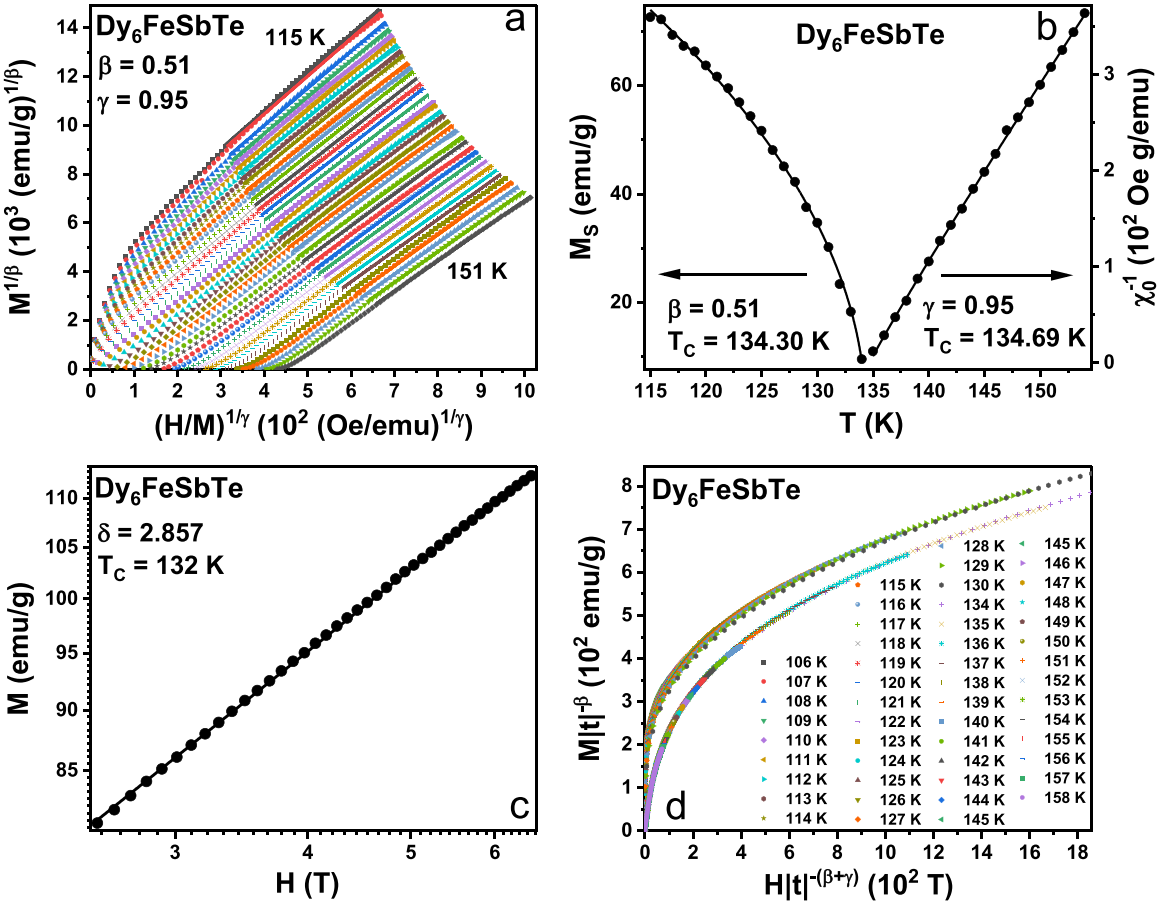

Fig. 8. $Dy_6FeSbTe$: a) Optimized Modified Arrot Plot; b) Spontaneous magnetization (left) and inverse of initial susceptibility (right) vs. temperature after Eqs. (1, 2); c) M vs. H plot in a log-log scale collected at the critical isotherm, after Eq. (3); d) The renormalized magnetization plotted as a function of the renormalized field, after Eq. (4).

Table 3
Critical exponents obtained for $Dy_6(Fe, Mn)X_2$ (X=Sb, Bi,Te).

Material	Technique	β	γ	δ
Dy_6FeBi_2	Modified Arrott Plot	0.74 ± 0.03	0.774 ± 0.004	2.04[a] ± 0.04
	Critical Isotherm			2.025 ± 0.002
$Dy_6Fe_{0.5}Mn_{0.5}Bi_2$	Modified Arrott Plot	0.761 ± 0.008	1.00 ± 0.02	2.31[a] ± 0.04
	Critical Isotherm			2.312 ± 0.001
Dy_6MnBi_2	Modified Arrott Plot	0.522 ± 0.005	0.93 ± 0.02	2.79[a] ± 0.05
	Critical Isotherm			2.786 ± 0.001
Dy_6FeSb_2	Modified Arrott Plot	0.72 ± 0.02	0.85 ± 0.01	2.17[a] ± 0.04
	Critical Isotherm			2.188 ± 0.007
$Dy_6FeSbBi$	Modified Arrott Plot	0.77 ± 0.02	0.776 ± 0.004	2.00[a] ± 0.03
	Critical Isotherm			2.008 ± 0.003
$Dy_6FeSbTe$	Modified Arrott Plot	0.51 ± 0.01	0.95 ± 0.02	2.87[a] ± 0.07
	Critical Isotherm			2.857 ± 0.007
$Dy_6FeBiTe$	Modified Arrott Plot	0.82 ± 0.06	0.93 ± 0.04	2.1[a] ± 0.1
	Critical Isotherm			2.135 ± 0.006

[a] Calculated from Eq. (5) $\delta = 1 + \gamma/\beta$.

role of the X element is to improve $|\Delta S_M^{pk}|$. In this sense, Sb and Te give better results than Bi, specially the first one.

As already mentioned in Section 3.2, it is commonly accepted that, in the family R_6TX_2, the rare earth atoms are solely responsible for the magnetic properties. This is due to the fact that no magnetic moment from T has been found in the cases where neutron diffraction studies have been undertaken [26,30–32,56–58]; rare earth ions interact through an indirect *4f-4f* interaction via the Ruderman-Kittel-Kasuya-Yosida (RKKY) interaction mediated by the *d*-band, which is sensitive to the position of the ions in the cell and the possible orbital hybridizations among the ions in the compound. In order to formulate an interpretation on why the different ion substitutions produce such changes in the magnetic and magnetocaloric properites, ab initio calculations should be performed to compare theoretical predictions with the experiments. This will be the purpose of a future work.

It is worth mentioning that, as seen in the previous section, the presence of small secondary phases in some intermetallics do not have a relevant influence on the magnetic entropy change as the features appearing in Fig. 9 are directly linked to the magnetic transitions of the main phases.

Another relevant property to characterize the suitability of a magnetocaloric material is the refrigerant capacity. This is traditionally calculated by means of RC_{FWHM} (which is obtained multiplying the width of the magnetic entropy change at half maximum times the value of the peak), or RC_{Area} (which is defined as the area enclosed by the magnetic entropy change vs. temperature curve in the range enclosed by the full width at half maximum). Nevertheless, there is a growing current in literature which disputes the suitability of these variables to ascertain the magnetocaloric quality of the materials when the peak is too wide or the temperature span gets enlarged by the presence of several transitions, which is our case, and, instead, proposes the use of the Temperature Average Entropy Change $TEC(10)$, which is defined as

$$TEC(10) = \frac{1}{10}\int_{T-5}^{T+5} \Delta S_{iso}(T')dT' \tag{7}$$

in order to avoid the artificially large refrigerant capacity of shallow peaks [59,60].

This *TEC(10)* has been thus chosen to evaluate the magnetocaloric properties and Fig. 10 collects the result of the DMCE in the shape of circles. Their centers are placed at the value of the maxima of the magnetic entropy change and their diameters are proportional to the value of $TEC(10)$. The values for the other rare earth high entropy compounds (grey circles) have been elaborated after [60,61], for comparison.

It is clear from Fig. 10 that two Sb-containing compounds (Dy_6FeSb_2 and $Dy_6FeSbTe$) are the ones with competitive properties with respect to other rare earth compounds. It is worth stressing the point that there is neither magnetic nor thermal hysteresis in the transitions, which is relevant for practical applications. Besides, the broad temperature range of application is an interesting issue, especially when considering an Ericsson cycle of refrigeration.

Moreover, if we look at the values of the maximum of the magnetic entropy change in the IMCEs (Fig. 8) we can see that for some compounds ($Dy_6FeSbBi$, $Dy_6FeSbTe$, $Dy_6FeBiTe$, Dy_6FeBi_2) they are indeed competitive for very low temperature applications, below 15–10 K. This could be interesting on its own for refrigeration in this range or to be used as heat-sinks for heat generated when a conventional magnetocaloric material is magnetized by adiabatic demagnetization before cooling [62]. As this IMCE is related to the metamagnetic transition, it is first order so the hysteresis could be an issue. It has not been possible to evaluate the TEC for these IMCE as the peaks are not complete. Another possible applications of these materials has to do with the fact that the refrigeration efficiency can be improved using materials with adjoint IMCE and DMCE [63].

The magnetocaloric variables, for the case of second order phase transitions, also fulfill some scaling equations which allow to reinforce the results obtained in the previous section for the PM-FM transition in each composition. The peak maximum of the magnetic entropy change scales as:

$$\Delta S_M^{pk} \sim H^n \tag{8}$$

where n is related to the previously defined (β, δ)

$$n = 1 + (1/\delta)(1 - 1/\beta) \tag{9}$$

Fig. 11 shows how Eq. (8) is very well fulfilled with an n calculated using the values of (β, δ) contained in Table 3, for the case of Dy_6MnBi_2 and Dy6FeSbBi (it is similar with all the rest). In the figure, the experimental points fall along a straight line, confirming the validity of the critical exponents.

Finally, let's check the possibility of obtaining the so called "magnetocaloric master curves" or "universal curves" for each composition around T_C [64]. A normalization of the variation of the magnetic entropy change for each field with respect to the corresponding maximum value, together with rescaling the temperature axis, should lead to a collapse of all points onto one single curve, in the critical region. The temperature axis rescaling can be done with one or two reference temperatures T_{r1}, T_{r2}, two being necessary when demagnetization effects are not negligible [65], as it happens in this case. The temperature axis is rescaled following:

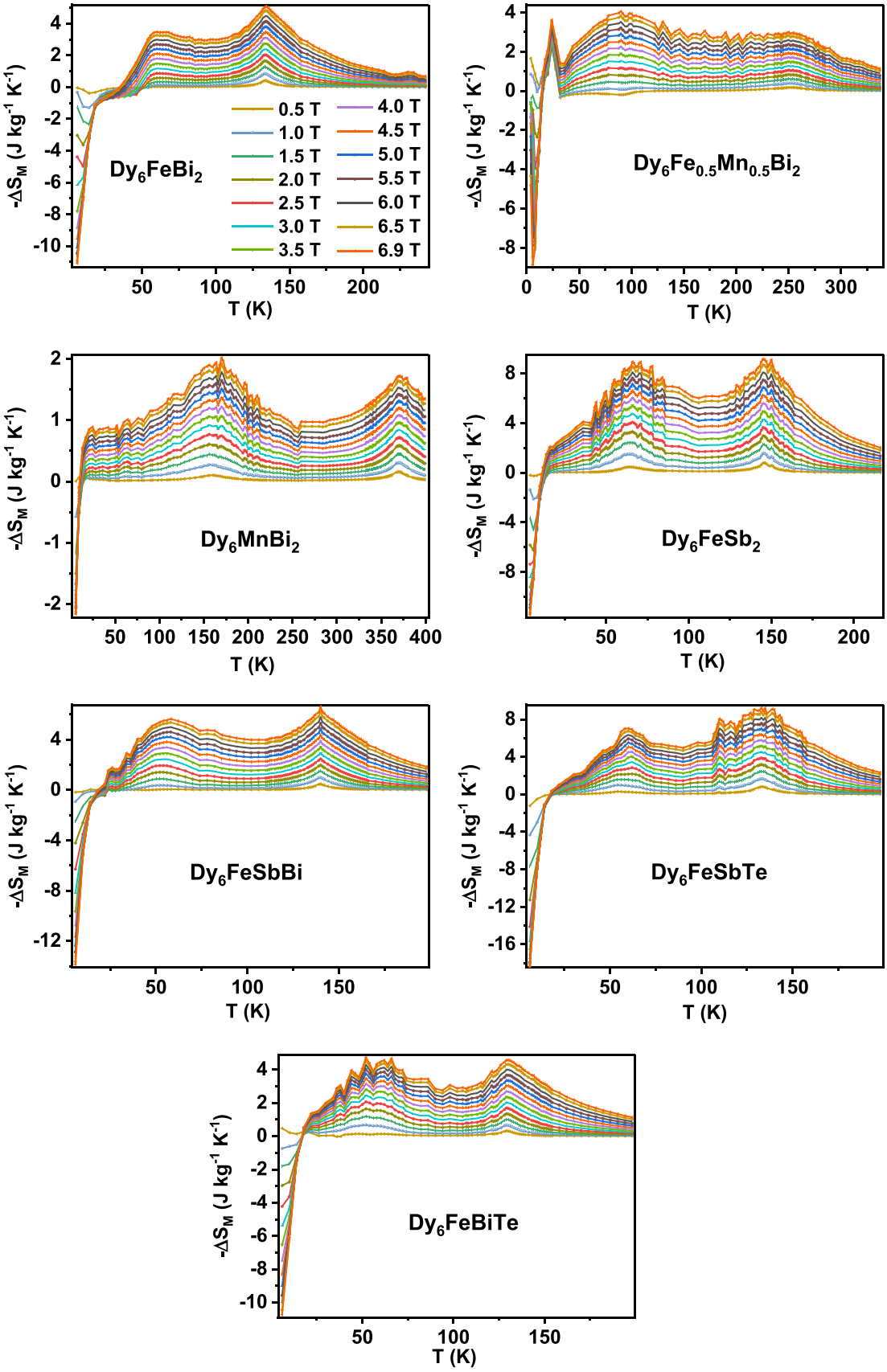

Fig. 9. Magnetic entropy change -ΔS_M for $\mu_0 \Delta H$ from 1 T to 6.9 T. The color code is the same for all of them.

Table 4
Magnitude of the magnetic entropy change $|\Delta S_M^{pk}|$ at different applied fields $\mu_0\Delta H$ (2, 5 and 6.9 T) for $Dy_6(Fe, Mn)X_2$ (X=Sb, Bi,Te). The indicated temperatures correspond to the position of the maximum of $-\Delta S_M$.

		Material							
		Dy_6FeBi_2 T_m= 60 K T_C= 134 K	$Dy_6Fe_{0.5}Mn_{0.5}Bi_2$ T_m= 90 K T_C= 250 K	Dy_6MnBi_2 T_m= 170 K T_C= 370 K	Dy_6FeSb_2 T_m= 66 K T_C= 145 K	$Dy_6FeSbBi$ T_m ≈ 56 K T_C= 140 K	$Dy_6FeSbTe$ T_m= 60 K T_C= 133 K	$Dy_6FeBiTe$ T_m= 52 K T_C= 129 K
2 T	$\lvert\Delta S_M^{pk}\rvert$ (J kg^{-1} K^{-1}) [T_m]	0.6	0.8	0.6	3.3	1.4	2.2	1.7
	$\lvert\Delta S_M^{pk}\rvert$ (J kg^{-1} K^{-1}) [T_C]	1.7	0.8	0.6	3.0	2.0	3.2	1.4
5 T	$\lvert\Delta S_M^{pk}\rvert$ (J kg^{-1} K^{-1}) [T_m]	2.4	2.9	1.5	7.1	4.2	5.5	3.8
	$\lvert\Delta S_M^{pk}\rvert$ (J kg^{-1} K^{-1}) [T_C]	3.8	2.2	1.3	6.9	4.8	7.0	3.4
6.9 T	$\lvert\Delta S_M^{pk}\rvert$ (J kg^{-1} K^{-1}) [T_m]	3.47	4.1	2.0	8.9	5.7	7.0	4.7
	$\lvert\Delta S_M^{pk}\rvert$ (J kg^{-1} K^{-1}) [T_C]	5.1	3.0	1.7	9.2	6.6	9.2	4.6

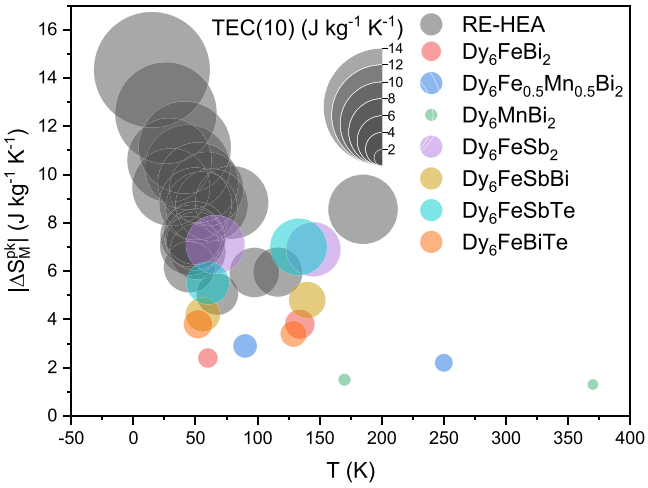

Fig. 10. DMCE performance at $\mu_0\Delta H$ = 5 T studied in this work and for selected rare earth high entropy alloys (RE-HEA) found in literature [60,61].

$$\theta_2 = \begin{cases} -(T - T_C)/(T_{r1} - T_C), & T \le T_C \\ (T - T_C)/(T_{r2} - T_C), & T > T_C \end{cases} \tag{10}$$

Fig. 12 shows, as an example, the universal curves thus obtained for Dy_6FeBi_2 and $Dy_6FeSbBi$, where the superposition is very good, as theory ascertains for the near vicinity of the second order phase transition [66], where critical theory is fulfilled. On the left hand side, at temperatures well below T_C, and due to the presence of the spin-reorientation transition, the theory does not hold and, therefore, the superposition is not good. The curves are similar in all the rest, except for $Dy_6Fe_{0.5}Mn_{0.5}Bi_2$ where, as commented before, the shape of the curve in the low temperature side makes it impossible to separate the part which corresponds to the critical region.

The fact that these master curves have been built is another strong support of the second order character of the PM-FM transition.

3.5. Thermal diffusivity

Heat exchange in a magnetic refrigerator implies that the thermal properties of the magnetocaloric material must be properly optimized in order to allow high working frequencies [3,16]. As temperature is changing in the material while it follows the cycles in the refrigerator, the equation which reflects heat transfer in that non-steady situation is:

$$\nabla^2 T(\vec{r}, t) + \frac{g(\vec{r}, t)}{K} = \frac{1}{D}\frac{\partial T(r, t)}{\partial t} \tag{11}$$

where $T(\mathbf{r},t)$ is the temperature field as a function of the position vector and time, $g(\mathbf{r},t)$ is the heat generated in the medium per unit time and unit volume, K is the thermal conductivity and D is the thermal diffusivity of the material, which characterizes how fast heat is transferred in the material [67]. D is related to other thermal properties by the following equation

$$D = \frac{K}{\rho c_p} \tag{12}$$

where c_p is the specific heat and ρ the density.

Fig. 13 shows the evolution of the thermal diffusivity in the regions of interest corresponding to the DMCEs. As intermetallic materials, the values are in the range 1–3 mm^2/s, which are comparable to the values exhibited by good magnetocaloric materials such as

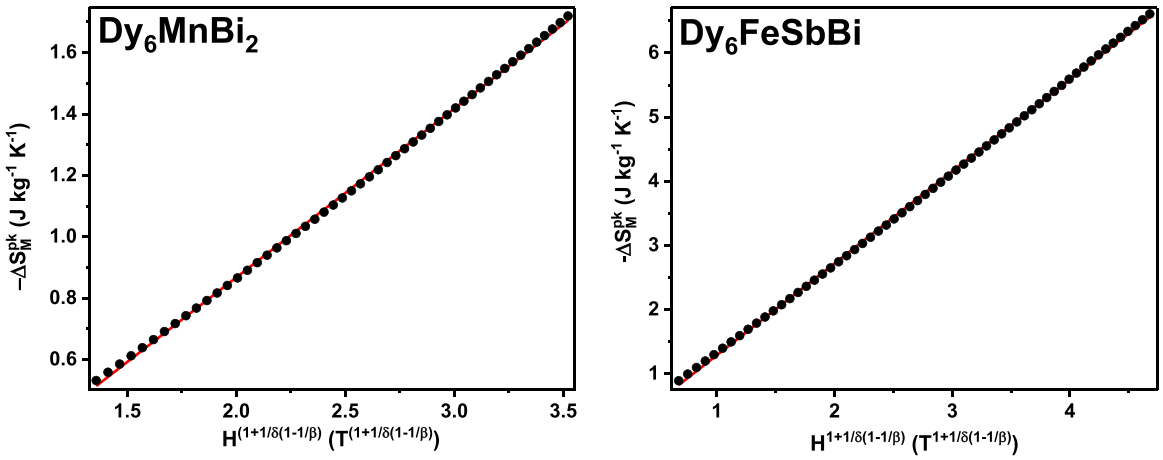

Fig. 11. Field dependences of the peak magnetic entropy change for Dy_6MnBi_2 (left) $Dy_6FeSbBi$ (right). The values of β and δ for each case are the ones presented in Table 3.

$Gd_5Si_2Ge_2$, $La(Fe_{0.88}Si_{0.12})_{13}$ and one order of magnitude higher than the case of MnAs [16].

The shape of the thermal diffusivity curves in intermetallic materials share several common features, which have to do with the fact that heat is transferred both by electrons and phonons, the contribution of the latter becoming more relevant at low temperatures [68,69]. Starting from high temperature, in the paramagnetic phase, while there is no magnetic transitions as temperature is decreased, the common behavior is to have a monotonic decrease in D (see in Fig. 13 the cases of the five compounds without Mn) due to the reduction of the electronic contribution, after the Wiedemann-Franz law [70]. Then the PM-FM transition takes place which is signalled as a dip (this is quite common both in metallic and insulator materials [21,71]). After this ordering, the phonon mean free path starts to increase and, depending on the leverage of the electronic and phononic contribution, different temperature dependencies arise between the PM-FM and the spin reorientation transition, which is in the region of the second dip. From then on, the phonon contribution dominates and as the phonon mean free path becomes larger and larger with the temperature decrease, a quick increase in D takes place. On the other hand, it is worth mentioning that in all samples which present small percentages of secondary phases, there is no signature of clear phase transitions associated with them, revealing that they do not play a relevant role.

In Dy_6MnBi_2, as the PM-FM transition takes place at a much higher temperature than the rest, the increase in the phononic contribution starts to compensate earlier the decrease in the electronic part. Finally, $Dy_6Fe_{0.5}Mn_{0.5}Bi_2$, presents an intermediate behavior between Dy_6MnBi_2 and Dy_6FeBi_2.

In all cases, detailed measurements in heating and cooling runs have shown that there is no thermal hysteresis at zero field and that the PM-FM transitions, as well as the spin reorientation ones at lower temperatures are, indeed, second order, emphasizing the absence of hysteresis in the DMCE regions.

Finally, the specific heat has also been measured at room temperature for all samples (159.9 J/kgK for Dy_6FeBi_2, 174.7 J/kgK for $Dy_6Fe_{0.5}Mn_{0.5}Bi_2$, 181.2 J/kgK for Dy_6MnBi_2, 197.7 J/kgK for Dy_6FeSb_2, 181.0 J/kgK for $Dy_6FeSbBi$, 190.1 J/kgK for $Dy_6FeSbTe$, and 184.5 J/kgK for $Dy_6FeBiTe$). This variable is relevant to evaluate the use of these materials as heat sinks, though it would be desirable to evaluate them near the magnetic transitions. Unfortunately, there is very scarce information in literature to make a good comparison with other magnetocaloric materials, save for a selection presented in [3]. If we convert these values to molar heat capacity per atom, they are between 25.74 and 29.15 J/molK per atom (between 3.1 R and 3.5 R, being R the universal gas constant), with results close to the ones given by the Dulong and Petit law (3 R), and in the common range for rare earth atoms.

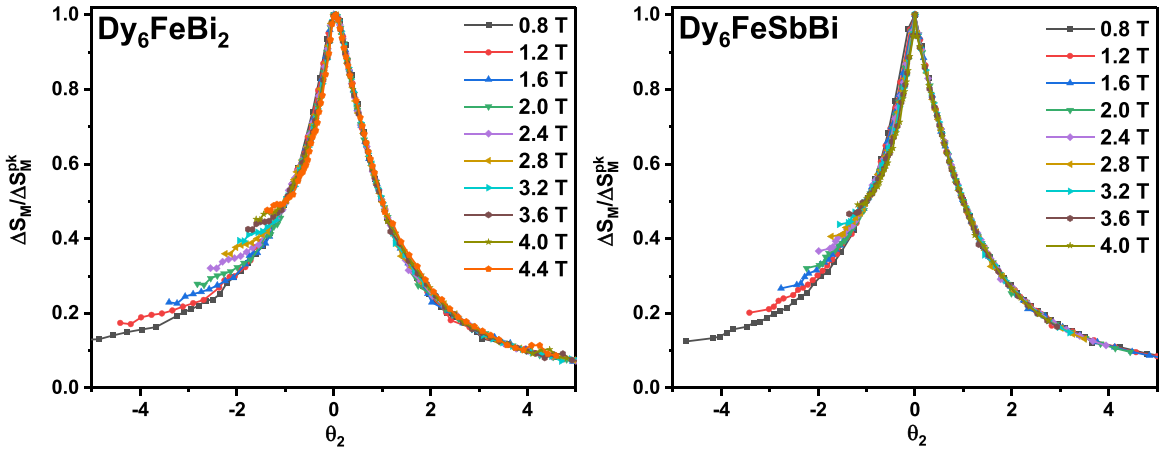

Fig. 12. Universal curve with the rescaled magnetic entropy changes using two reference temperatures, for Dy_6FeBi_2 and $Dy_6FeSbBi$.

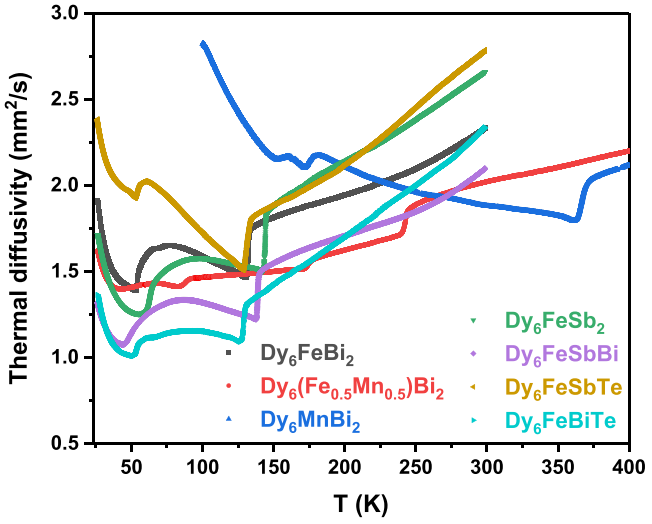

Fig. 13. Thermal diffusivity curves for Dy_6FeBi_2, $Dy_6Fe_{0.5}Mn_{0.5}Bi_2$, Dy_6MnBi_2, Dy_6FeSb_2, $Dy_6FeSbBi$, $Dy_6FeSbTe$, and $Dy_6FeBiTe$.

4. Conclusions

The $Dy_6(Fe,Mn)X_2$ (X=Sb, Bi, Te) family of intermetallics has been thoroughly studied, characterizing different properties. They all crystallize in the Fe_2P-type structure (space group $P\bar{6}2m$) and share common magnetic properties in the succession of magnetic transitions that appear while lowering the temperature from the paramagnetic phase. First, a paramagnetic to ferromagnetic transition (in the range 129–370 K), followed by a spin-reorientation one (from 52 to 170 K). Then, at very low temperature, a complex ground magnetic state is reached, with antiferromagnetic components. The latter is taken to a ferromagnetic one with applied magnetic fields, showing metamagnetic transitions. This complexity gives rise to two DMCE and one IMCE in all compounds, where there is a table-like effect between the two DMCE, a requirement for improving the efficiency of an Ericsson cycle refrigerant; the advantage is that this table-like effect is obtained by using a single material instead of the usual method of building a composite material. Furthermore, the position and height of this region can be efficiently tuned varying the composition. The Sb-containing (Dy_6FeSb_2 and $Dy_6FeSbTe$) have the best magnetocaloric properties among the compounds studied, with moderate values of the magnetic entropy maxima $|\Delta S_M^{pk}|$ and *TEC(10)* values well placed among rare earth based high entropy alloys. The IMCE that all compounds show is again specially relevant for the ones containing Sb. The critical behavior analysis performed on the PM-FM transitions, with the calculation of the critical exponents β,γ,δ suggests that long-range order interactions are responsible for these magnetic transitions, though only in two cases (Dy_6MnBi_2 and $Dy_6FeSbTe$) the values agree with the Mean Field universality class. The rest present an unconventional critical behavior as the values of β are too high or the values of γ too low to comply with an already theorized universality class. There is agreement between these values and the scaling of the magnetocaloric variable ΔS_M^{pk} and the obtention of the universal curves. Finally, the thermal transport properties (thermal diffusivity) present high enough values for these compounds to be considered as candidates for real magnetocaloric refrigeration systems.

CRediT authorship contribution statement

A. Herrero: Investigation, Software, Formal analysis, Validation, Writing – original draft. **A. Oleaga:** Supervision, Conceptualization, Methodology, Formal analysis, Validation, Writing – original draft, Writing – review & editing. **I.R. Aseguinolaza:** Investigation, Formal analysis. **A. Garcia-Adeva:** Investigation, Formal analysis. **E. Apiñaniz:** Investigation, Formal analysis. **A.V. Garshev:** Investigation, Formal analysis. **V.O. Yapaskurt:** Investigation, Formal analysis. **A.V. Morozkin:** Conceptualization, Investigation, Formal analysis, Writing – review & editing.

Declaration of Competing Interest

The authors declare that they have no known competing financial interests or personal relationships that could have appeared to influence the work reported in this paper.

Acknowledgements

This work has been supported by Universidad del País Vasco UPV/EHU (project GIU19/058) and the Russian Fund for Basic Research (project N° 20-03-00209-a). A. Herrero thanks the Department of Education of the Basque Government as grantee of the programme “Programa Predoctoral de Formación de Personal Investigador No Doctor”. The authors thank for technical and human support provided by SGIker of UPV/EHU, specially the fruitful discussions with Dr. I. Orue.

Appendix A. Supporting information

Supplementary data associated with this article can be found in the online version at doi:10.1016/j.jallcom.2021.161849.

References

[1] O. Gutfleisch, M.A. Willard, E. Brück, C.H. Chen, S.G. Sankar, J.P. Liu, Magnetic materials and devices for the 21st century: stronger, lighter, and more energy efficent, Adv. Mater. 23 (2011) 821–842.
[2] V. Franco, J.S. Blázquez, J.J. Ipus, J.Y. Law, L.M. Moreno-Ramírez, A. Conde, Magnetocaloric effect: From materials research to refrigeration devices, Prog. Mat. Sci. 93 (2018) 112–232.
[3] T. Gotschall, K.P. Skokov, M. Fries, A. Taubel, I. Radulov, F. Scheibel, D. Benke, S. Riegg, O. Gutfleisch, Making a cool choice: the materials library of magnetic refrigeration, Adv. Energy Mater. 9 (2019) 1–13 1901322.
[4] Y. Zhang, Review of the structural, magnetic and magnetocaloric properties in ternary rare earth RE_2T_2X type intermetallic compounds, J. Alloy. Compd. 787 (2019) 1173–1186.
[5] H. Zhang, R. Gimaev, B. Kovalev, K. Kamilov, V. Zverev, Review on the materials and devices for magnetic refrigeration in the temperature range of nitrogen and hydrogen liquefaction, Phys. B: Condens. Matter 558 (2019) 65–73.
[6] L.W. Li, Review of magnetic properties and magnetocaloric effect in the intermetallic compounds of rare earth with low boiling point, Chin. Phys. B 25 (2016) 037502.
[7] K.A. Gschneidner Jr., V.K. Pecharsky, A.O. Tsokol, Recent developments in magnetocaloric materials, Rep. Prog. Phys. 68 (2005) 1479–1539.
[8] L. Li, M. Yan, Recent progresses in exploring the rare earth based intermetallic compounds for cryogenic magnetic refrigeration, J. Alloy. Compd. 823 (2020) 153810.
[9] M. Balli, S. Jandl, P. Fournier, A. Kedous-Lebouc, Advanced materials for magnetic cooling: Fundamentals and practical aspects, Appl. Phys. Rev. 4 (2017) 021305.
[10] A. Fujita, S. Fujieda, Y. Hasegawa, K. Fukamichi, Itinerant-electron metamagnetic transition and large magnetocaloric effects inLa(FexSi1−x)13compounds and their hydrides, Phys. Rev. B 67 (2003) 104416.
[11] H. Wada, T. Takahara, K. Katagiri, T. Ohnishi, K. Soejima, K. Yamashita, Recent progress of magnetocaloric effect and magnetic refrigerant materials of Mn compounds, J. Appl. Phys. 117 (2015) 172606.
[12] F. Chen, J.L. Sanchez Llamazares, C.F. Sanchez-Valdes, F. Chen, Z. Li, Y.X. Tong, L. Li, Large magnetic entropy change and refrigeration capacity around room temperature in quinary Ni41Co9-xFexMn40Sn10 alloys (x= 2.0 and 2.5), J. Alloy. Compd. 825 (2020) 154053.
[13] H. Zhang, Y.J. Sun, E. Niu, L.H. Yang, J. Shen, F.X. Hu, J.R. Sun, B.G. Shen, Large magnetocaloric effects of RFeSi (R = Tb and Dy) compounds for magnetic refrigeration in nitrogen and natural gas liquefaction, Appl. Phys. Lett. 103 (2013) 202412.
[14] A. Herrero, A. Oleaga, A. Salazar, A.V. Garshev, V.O. Yapaskurt, A.V. Morozkin, Magnetocaloric properties, magnetic interactions and critical behavior in $Ho_6(Fe,Mn)Bi_2$ intermetallics, J. Alloy. Compd. 821 (2020) 153198.
[15] A. Herrero, A. Oleaga, A. Salazar, A.V. Garshev, V.O. Yapaskurt, A.V. Morozkin, Magnetocaloric properties and unconventional critical behavior in $(Gd,Tb)_6(Fe,Mn)Bi_2$ intermetallics, J. Alloy. Compd. 843 (2020) 155937.
[16] S. Fujieda, Y. Hasegawa, A. Fujita, K. Fukamichi, Thermal transport properties of magnetic refrigerants $La(Fe_xSi_{1-x})_{13}$ and their hydrides, and $Gd_5Si_2Ge_2$ and MnAs, J. Appl. Phys. 95 (2004) 2429–2431.

[17] F. Izumi, R.A. Young (Ed.), The Rietveld Method, Oxford University Press, Oxford, 1993Chap. 13.
[18] V. Franco, J.Y. Law, A. Conde, V. Brabander, D.Y. Karpenkov, I. Radulov, K. Skokov, O. Gutfleisch, Predicting the tricritical point composition of a series of LaFeSi magnetocaloric alloys via universal scaling, J. Phys. D: Appl. Phys. 50 (2017) 414004.
[19] H. Neves Bez, H. Yibole, A. Pathak, Y. Mudryk, V.K. Pecharsky, Best practices in evaluation of the magnetocaloric effect from bulk magnetization measurements, J. Magn. Magn. Mater. 458 (2018) 301–309.
[20] W. Jiang, X.Z. Zhou, G. Williams, Y. Mukovskii, K. Glazyrin, Griffiths phase and critical behavior in single-crystalLa0.7Ba0.3MnO3: Phase diagram forLa1−xBaxMnO3(x⩽0.33), Phys. Rev. B 77 (2008) 064424.
[21] A. Oleaga, A. Salazar, D. Prabhakaran, J.G. Cheng, J.S. Zhou, Critical behavior of the paramagnetic to antiferromagnetic transition in orthorhombic and hexagonal phases of $RMnO_3$ (R = Sm, Tb, Dy, Ho, Er, Tm, Yb, Lu, Y), Phys. Rev. B 85 (2012) 184425.
[22] A.V. Morozkin, New Zr_6CoAs_2-type R_6FeSb_2 (R=Sc, Y, Lu, Dy, Ho, Tm) and Ho6FeBi2 compounds, J. Alloy. Compd. 353 (2003) L16–L18.
[23] A.V. Morozkin, New Zr_6CoAs_2-type R_6FeBi_2 (R=Y, Lu, Gd-Dy, Er, Tm, J. Alloy. Compd. 358 (2003) L9–L10.
[24] A.V. Morozkin, New Zr_6CoAs_2-type R_6MnSb_2 and R_6MnBi_2 compounds (R=Y, Lu, Dy, Ho), J. Alloy. Compd. 360 (2003) L1–L2.
[25] A.V. Morozkin, Yu Mozharivskyj, V. Svitlyk, R. Nirmala, A.K. Nigam, Magnetic properties of Fe_2P-type Tb_6FeTe_2, Tb_6CoTe_2, Tb_6NiTe_2 and Er_6FeTe_2 compounds, J. Solid State Chem. 183 (2010) 3039–3051.
[26] A.V. Morozkin, R. Nirmala, S.K. Malik, Structural and magnetic properties of Fe_2P-type R_6TX_2 compounds (R = Zr, Dy, Ho, Er, Tj Mn, Fe, Co, Cu, Ru, Rh, X = Sb, Bi, Te), Intermetallics 19 (2011) 1250–1264.
[27] Springer Materials The Landolt-Börnstein Database - Materials Science Data for 250000 Substances, ⟨http://www.springermaterials.com⟩.
[28] A. Herrero, A. Oleaga, A. Provino, I.R. Aseguinolaza, A. Salazar, D. Peddis, P. Manfrinetti, Crystallographic, magnetic and magnetocaloric properties in novel intermetallic materials R_3CoNi (R = Tb, Dy, Ho, Er, Tm, Lu), J. Alloy. Compd. 865 (2021) 158948.
[29] A.V. Morozkin, Magnetic structures of Zr6CoAs2-type Ho6FeSb2, Ho6CoBi2, Ho6FeBi2 and Ho6MnBi2 compounds, J. Alloy. Compd. 395 (2005) 7–16.
[30] A.V. Morozkin, V.N. Nikiforov, B. Malaman, Magnetic structure of the Zr_6CoAs_2-type Tb_6FeBi_2 compound, J. Alloy. Compd. 393 (2005) L6–L9.
[31] A.V. Morozkin, Yu Mozharivskyj, V. Svitlyk, R. Nirmala, O. Isnard, P. Manfrinetti, A. Provino, C. Ritter, Magnetic properties of Fe_2P-type R_6CoTe_2 compounds (R=Gd–Er), J. Solid State Chem. 183 (2010) 1314–1325.
[32] A.V. Morozkin, O. Isnard, P. Manfrinetti, A. Provino, C. Ritter, R. Nirmala, S.K. Malik, The magnetic ordering in the Ho_6FeTe_2, J. Alloy. Compd. 498 (2010) 13–18.
[33] A.V. Morozkin, O. Isnard, P. Henry, P. Manfrinetti, R. Nirmala, S.K. Malik, Magnetic structures of Zr_6CoAs_2-type $Ho_{6-x}Er_xMnBi_2$ solid solutions, J. Alloy. Compd. 450 (2008) 62–74.
[34] M. Drzyzga, J. Szade, Structure and magnetism of R_5Bi_3 (R=Tb, Dy, Ho, Er) and Tb_4Bi_3, J. Alloy. Compd. 321 (2001) 27–34.
[35] I.P. Semitelou, P. Kotsanidis, J.K. Yakinthos, E. Roudaut, The sine-modulated magnetic structure of Dy_5Sb_3, J. Magn. Magn. Mater. 116 (1992) 103–107.
[36] S.K. Banerjee, On a generalized approach to first and second order magnetic transitions, Phys. Lett. 12 (1964) 16–17.
[37] H.E. Stanley, Introduction to phase transitions and critical phenomena, Oxford University Press, 1971.
[38] M. Campostrini, M. Hasenbusch, A. Pelissetto, P. Rossi, E. Vicari, 25th-order high-temperature expansion results for three-dimensional Ising-like systems on the simple-cubic lattice, Phys. Rev. E Stat. Nonlin Soft Matter Phys. 65 (2002) 066127.
[39] M. Campostrini, A. Pelisseto, P. Rossi, E. Vicari, 25-th order high-temperature expansion results for three-dimensional Ising-like systems on the simple-cubic lattice, Phys. Rev. E 65 (2002) 066127.
[40] M. Campostrini, M. Hasenbusch, A. Pelisseto, P. Rossi, E. Vicari, Critical behavior of the three-dimensional XY universality class, Phys. Rev. B 63 (2001) 214503.
[41] H. Kawamura, Universality of phase transitions of frustrated antiferromagnets, J. Phys.: Condens. Matter 10 (1998) 4707.
[42] E.K. Riedel, F.J. Wegner, Tricritical Exponents and Scaling Fields, Phys. Rev. Lett. 29 (1972) 349–352.
[43] J.C. LeGuillou, J. Zinn-Justin, Critical exponents from field theory, Phys. Rev. B 221 (1980) 3976–3998.
[44] Y. Liu, C. Petrovic, Critical behavior of the quasi-two-dimensional weak itinerant ferromagnet trigonal chromium telluride $Cr_{0.62}Te$, Phys. Rev. B 96 (2017) 134410.
[45] A.T. Ogielski, Dynamics of three-dimensional Ising spin glasses in thermal equilibrium, Phys. Rev. B Condens Matter 32 (1985) 7384–7398.
[46] M.E. Fisher, S.K. Ma, B.G. Nickel, Critical exponents for long-range order interactions, Phys. Rev. Lett. 29 (1972) 917–920.
[47] J. Jensen, A.R. Macintosh, Rare Earth Magnetism: Structures and Excitations, Clarendon Press, Oxford, 1991.
[48] F. Kagawa, K. Miyagawa, K. Kanoda, Unconventional critical behaviour in a quasi-two-dimensional organic conductor, Nature 436 (2005) 534–537.
[49] T. Kida, A. Senda, S. Yoshii, M. Hagiwara, T. Takeuchi, T. Nakano, I. Terasaki, Unconventional critical behavior in the weak ferromagnet BaIrO3, EPL (Europhys. Lett.) 84 (2008) 27004.
[50] Y. Yin, J.C. Han, Q. Yuan, L.S. Ling, B. Song, Critical behaviour in the antiperovskite Mn_3CuN at ferromagnetic to paramagnetic phase transition, J. Magn. Magn. Mater. 346 (2013) 203–208.
[51] A. Omerzu, M. Tokumoto, B. Tadić, D. Mihailovic, Critical exponents at the ferromagnetic transition in tetrakis(dimethylamino)ethylene-C(60) (TDAE- C(60)), Phys. Rev. Lett. 87 (2001) 177205.
[52] Y. Itoh, T. Mizoguchi, K. Yoshimura, Novel critical exponent of magnetization curves near the ferromagnetic quantum phase transitions of Sr1-xAxRuO3(A = Ca, La0.5Na0.5, and La), J. Phys. Soc. Jpn. 77 (2008) 123702.
[53] D. Fuchs, M. Wissinger, J. Schmalian, C.-L. Huang, R. Fromknecht, R. Schneider, Critical scaling analysis of the itinerant ferromagnetSr1−xCaxRuO3, Phys. Rev. B 89 (2014) 174405.
[54] M. Triki, E. Dhahri, E.K. Hlil, Unconventional critical magnetic behaviour in the Griffiths ferromagnet $La_{0.4}Ca_{0.6}MnO_{2.8}$, $_{0.2}$ oxide, J. Sol. State Chem. 201 (2013) 63–67.
[55] N. Assoudi, M. Smari, I. Walha, E. Dhahri, S. Shevyrtalov, O. Dikaya, V. Rodionova, Unconventional critical behavior near the phase transition temperature and magnetocaloric effect in $La_{0.5}Ca_{0.4}Ag_{0.1}MnO_3$ compound, Chem. Phys. Lett. 706 (2018) 182–188.
[56] J. Zhang, G. Shan, Z. Zheng, C.H. Shek, Structure and magnetic behaviors of Gd_6FeBi_2 compound, Intermetallics 68 (2016) 51–56.
[57] J. Zhang, Y.M. Kang, G. Shan, S. Bobev, Structural analysis of Gd_6FeBi_2 from single-crystal X-ray diffraction methods and electronic structure calculations, Acta Crystallogr. C 75 (2019) 562–567.
[58] A.V. Morozkin, R. Nirmala, S.K. Malik, Magnetic structure of the Zr_6CoAs_2-type Er_6TX_2 compounds (T= Mn, Fe, Co and X=Sb, Bi), J. Alloy. Compd. 394 (2005) 75–79.
[59] L.D. Griffith, Y. Mudryk, J. Slaughter, V.K. Pecharsky, Material-based figure of merit for caloric materials, J. Appl. Phys. 123 (2018) 034902.
[60] J.Y. Law, A. Diaz-Garcia, L.M. Moreno-Ramirez, V. Franco, Increased magnetocaloric response of FeMnNiGeSi high-entropy alloys, Acta Mater. 212 (2021) 116931.
[61] J.Y. Law, L.M. Moreno-Ramirez, A. Diaz-Garcia, A. Martin-Cid, S. Kobayashi, S. Kawaguchi, T. Nakamura, V. Franco, MnFeNiGeSi high-entropy alloy with large magnetocaloric effect, J. Alloy. Compd. 855 (2021) 157424.
[62] T. Krenke, E. Duman, M. Acet, E.F. Wassermann, X. Moya, L. Mañosa, A. Planes, Inverse magnetocaloric effect in ferromagnetic Ni-Mn-Sn alloys, Nat. Mater. 4 (2005) 450–454.
[63] L.V.B. Diop, O. Isnard, Inverse and normal magnetocaloric effects in $LaFe_{12}B_6$, J. Appl. Phys. 119 (2016) 213904.
[64] V. Franco, A. Conde, J.M. Romero-Enrique, J.S. Blázquez, A universal curve for the magnetocaloric effect: an analysis based on scaling relations, J. Phys. Condens. Matter 20 (2008) 285207.
[65] V. Franco, J.S. Blázquez, A. Conde, Field dependence of the magnetocaloric effect in materials with a second order phase transition: a master curve for the magnetic entropy change, Appl. Phys. Lett. 89 (2006) 222512.
[66] C. Romero-Muñiz, R. Tamura, S. Tanaka, V. Franco, Applicability of scaling behavior and power laws in the analysis of the magnetocaloric effect in second-order phase transition materials, Phys. Rev. B 94 (2016) 134401.
[67] A. Salazar, On thermal diffusivity, Eur. J. Phys. 24 (2003) 351–358.
[68] H. Misiorek, J. Stepién-Damma, W. Suski, E. Talik, B.Y. Kotur, V.M. Dmitriev, Lattice parameters, magnetic susceptibility and thermal conductivity of $ScFe_4Al_8$ and YFe_4Al_8, J. Alloy. Compd. 363 (2004) 78–84.
[69] A.K. Bashir, M.-B.T. Tchokonté, A.M. Strydom, Electrical and thermal transport properties of $RECu_4Au$ compounds, RE = Nd, Gd, J. Magn. Magn. Mater. 414 (2016) 69–73.
[70] A. Kowalczyk, M. Falkowski, Thermal conductivity of $CeNiAl_4$ Kondo lattice, Intermetallics 37 (2013) 65–68.
[71] A. Herrero, A. Oleaga, P. Manfrinetti, A. Provino, A. Salazar, Critical behavior of the ferromagnetic transition in GdSc(Si,Ge) intermetallic compounds, Intermetallics 101 (2018) 64–71.